Korean J. Chem. Eng., 40(9), 2128-2137 (2023)
DOI: 10.1007/s11814-023-1404-4

pISSN: 0256-1115
eISSN: 1975-7220

Criteria for evaluating working fluids in loop gravity-assisted heat systems

Jianxun Chen*, Jinping Liu*,,***, Xiongwen Xu*,**,†, Lingjiao Liang*, and Yinhao Yu***

*School of Electric Power, South China University of Technology, Guangzhou 510640, China
**Guangdong Province Key Laboratory of Efficient and Clean Energy Utilization,
South China University of Technology, Guangzhou 510640, China
***State Key Laboratory of Subtropical Building Science, South China University of Technology,
Guangzhou 510640, China
(*Received 15 September 2022 • Revised 5 February 2023 • Accepted 24 February 2023*)

Abstract−A loop gravity-assisted heat pipe (LGHP) is characterized by passive heat dissipation and extensive application prospect. Dissimilar working fluids give rise to noticeable differences in their working performance (Critical heat flux (CHF)). Consequently, it is of great significance to evaluate the performance of LGHP working fluid for its design. In accordance with the basic theories of CHF and hydrodynamics, the pressure drop models of laminar, smooth turbulence, and completely rough turbulence flows were established, and an extensible two-phase composite property parameter was obtained. On this basis, the physical property parameter of transitional rough turbulent flow was also derived. Finally, as persuasively illustrated by the experimental results, there was almost a linear association between CHFs and the derived physical parameter. As a result, the physical parameters derived in this paper can be employed as favorable criteria for the selection of LGHP working fluid.

Keywords: Loop Gravity-assisted Heat Pipe, Property Parameter, Critical Heat Flux, Working Fluid

INTRODUCTION

With the speed development in the electronics industry, electronic devices, featured by multiple developmental trends such as miniaturization and high heat dissipation, are being increasingly used in a multitude of areas. As a consequence, it is of paramount importance to design cooling equipment with compact structure, trustworthy performance, flexible installation, and high heat transfer capacity [1-3]. While traditional forced-air cooling is limited and may be insufficient for meeting the high demands of future electronics, two-phase cooling is considered to be promising for the dissipation of high heat flux, and is already extensively used in multiple fields such as electronic cooling, energy recovery systems, aerospace, solar energy [4-8]. Owing to the latent heat of evaporation dominating the energy transfer process, two-phase cooling is highly efficient when compared with single-phase cooling [9,10]. Two-phase cooling devices with higher thermal conductivity (over 200 times) than that of copper have been proven to be satisfactory heat transfer devices [11].

Typically, liquid cooling systems require a pump to drive the circulation of the working fluid. The two-phase LGHP system, which is a type of phase-changing, passive, and indirect liquid cooling design, has been proven to be both viable and trustworthy in cooling electronic devices with high heat fluxes [12,13]. As depicted in Fig. 1, an LGHP system is made up of an evaporator, a rising tube, a condenser, and a falling tube. The working fluid evaporates in the evaporator and transfers the heat from the heating component to the condenser. Subsequently, the vapor flows through the rising tube and condenses in the condenser. Ultimately, the condensed liquid flows back through the falling tube to the evaporator by gravity. The counter flow of the liquid and the vapor does not exist as a consequence of the loop structure. Owing to the striking difference in the gravitational force acting upon the liquid and that acting upon the vapor, the coolant does not require any pump or capillary action; consequently, the system stability and reliability are tremendously heightened and the maintenance costs decrease. Nevertheless, a natural weakness of this type of system is the limited critical heat flux (CHF), which is limited by the difference of driving force and flow resistance of working fluid in LGHP. As a result, reinforcing the flow performance to ameliorate the CHF is extremely paramount for LGHPs.

In the LGHP, the working fluid is driven by the difference in the gravitational forces acting upon the liquid and vapor. As a consequence, the height difference between the condenser and the evaporator exerts noticeable influences on the heat transfer limit. With the augment of height difference between the condenser and evaporator, the driving force of the LGHP increases, and flow resistance of the working fluid also increases. Consequently, the heat transfer performance of the LGHP can only be improved within a certain height difference [14-16].

The heat transfer performance of the evaporator also affects the overall performance of the LGHP. Effective methods for reinforcing the heat transfer performance have been studied, including adopting working fluids with higher heat transfer efficiency and modifying the evaporating surface. Liu [17] used a water-based carbon nanotube suspension as the working fluid in a miniature thermosyphon. As evidently revealed in the research, the thermal performance was strengthened. Liter [18] reported that the pool boiling

†To whom correspondence should be addressed.
E-mail: epxwxu@scut.edu.cn

CHF was enhanced nearly three times by applying a modulated porous-layer coating. Rahmatollah [19] designed a loop thermosyphon for electronic cooling. Its evaporator is made of small pieces of copper, with several vertical channels and a heated area of 9.53 mm×9.53 mm. The CHF of this system reached 268.3 kW/m^2 using isobutane. Nevertheless, on account of its poor pressure resistance, this system cannot employ a working fluid with high evaporating pressure and is not suitable for the cooling of large electronic devices.

So far, most studies have focused attention on heat exchangers in LGHPs, while fewer have discussed the working fluids chosen. Generally, working pressure is a critical factor in heat transfer and flow processes. In line with the pool-boiling mechanism [20-22], higher boiling pressures are linked to smaller bubble departure diameters [23,24] and better heat transfer. Furthermore, a higher pressure creates a higher vapor density, thereby lessening the vapor flow resistance, which is of benefit in the gravity-assisted heat pipe systems. Hence, the working pressure has a paramount role in the circulation of the working fluid [25] and may be a criterion for selecting the working fluid. Franco et al. [26] conducted experiments with a loop heat pipe employing dissimilar working fluids, such as water and ethanol. As clearly demonstrated by their research findings, the limiting value of the mass flow rate is immensely affected by both the working pressure and the filling ratio. Chen [27] studied the heat transfer performance of SLGHP using different working fluids (methanol, ammonia, water) with different diameters and heat source temperatures and proposed a comprehensive evaluation standard, but the composite property parameter was not summarized. Randeep [28] studied the thermal performance of LHP which used water, ethanol and methanol as working, and proposed that water was the optimal working fluid by studying the influence of merit number. Guo [29] proposed a cryogenic loop heat pipe and studied the start-up characteristics and heat transfer performance by using different working fluids (nitrogen, neon, hydrogen), but did not propose a physical parameter to evaluate the working fluids.

Nonetheless, the correlation between working pressure and CHF has not been strictly proven. Herein, on the basis of the CHF theory and fluid mechanics, we combined the primary influencing factors in LGHP systems and established a mathematical model which outputs a dimensionless number X, and two-phase physical parameters of the working fluid, to estimate the system performance. Aside from that, the reliability of two-phase physical parameters and working pressure in choosing the optimal working fluid was tested experimentally.

THEORETICAL ANALYSIS FOR CHOOSING A WORKING FLUID

1. Flow Force Balance in LGHP

As clearly depicted in Fig. 1, the driving force of the LGHP system is generated by the different density between the liquid in the falling tube and the vapor/liquid mixture in the rising tube, which is always balanced with the total pressure drop. When the system reaches the CHF state, the falling tube from the condenser outlet to the evaporator inlet is filled with liquid, and the rising tube from the evaporator outlet to the condenser inlet is filled with vapor. The evaporator tends to dry out with the increment of the heating flux.

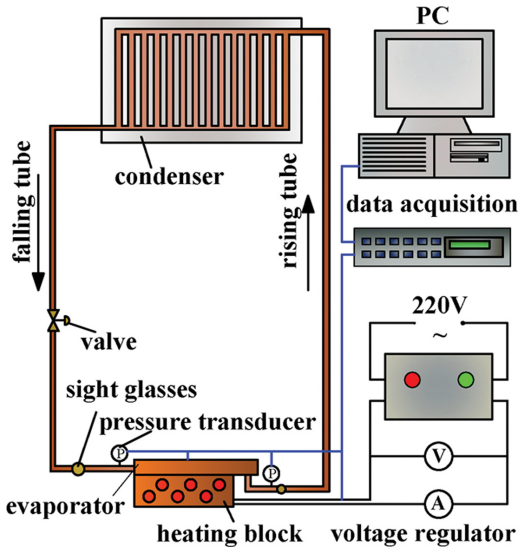

Fig. 1. Two-phase loop gravity-assisted heat pipe.

The temperature of the heating component will augment remarkably.

To study the critical state of an LGHP, the driving force of the working fluid should first be analyzed. In an LGHP system, the driving force can be described as the gravitational potential energy formed by the difference in density between the vapor (ρ_g) and the liquid (ρ_l), as depicted in Eq. (1):

$$\Delta p_t = (\rho_l - \rho_g)gH \tag{1}$$

where H is the vertical height difference of condenser and evaporator, g is the gravitational factor. In general, the latent heat of the working fluid plays a paramount role in the heat transfer process during the phase change process in an LGHP, and the sensible heat is usually negligible. Hence, the input heat is divided by the latent heat of evaporation to indicate the mass flow rate. While the system reaches the CHF, the mass flow rate ($\dot{m}$) of the working fluid can be determined by Eq. (2),

$$\dot{m} = \frac{Q}{\gamma} \tag{2}$$

where Q is the input heat power and γ is the latent heat of the working fluid. As the rising tube was filled with vapor when the system reached the CHF, the vapor velocity in the rising tube (u_1) was calculated using Eq. (3):

$$u = \frac{4\dot{m}}{\rho_g \pi d^2} \tag{3}$$

Since the density of the liquid is much greater than that of the vapor, the flow velocity of the working fluid in the falling tube is much slower than that in the rising tube. The single-phase pressure drop (Δp_g) is obtained by employing the Darcy-Wesbach formula, as displayed in Eq. (4) [30]:

$$\Delta p_g = f\frac{l_1}{d_1}\frac{\rho_g u^2}{2} \tag{4}$$

where l_1 is the length of the rising tube and d_1 is the inner diameter of the rising tube. The Reynolds number (Re) is calculated as dis-

Table 1. Calculation formulas of friction coefficients

Flow pattern	Calculation formula		Remark
Laminar flow	$f=\frac{64}{Re}$	(6)	
Smooth turbulent flow	$f=\frac{0.3164}{Re^{0.25}}$	(7)	Blasius formula
Transitional rough turbulent flow	$\frac{1}{\sqrt{f}}=-2.0\log\left(\frac{2.51}{Re\sqrt{f}}+\frac{\varepsilon/d}{3.7}\right)$	(8)	Cole Brook formula
Fully rough turbulent flow	$\frac{1}{\sqrt{f}}=-2.0\log\left(\frac{\varepsilon/d}{3.7}\right)$	(9)	von Karman formula

played in Eq. (5):

$$Re=\frac{\rho_g u d}{\mu_g} \tag{5}$$

The calculation of the friction coefficient f of an internal pipe flow can be divided into four cases in line with to the Re of the gaseous working fluid and listed in Table 1.

Analogous to the Darcy-Wesbach formula, the pressure drop (Δp_{gi}) in the evaporator, condenser and other parts of the LGHP can be calculated as follows:

$$\Delta p_{gi}=f_i\frac{l_i}{d_i}\frac{\rho_g u_i^2}{2} \tag{10}$$

where i represents the distinct parts of the system (1-rising tube, 2-condenser, 3-evaporator etc.).

2. Dimensionless Property Quantity

With regard to a given working fluid, the maximum driving force in the system is equivalent to the total pressure (Δp_t, as illustrated in Eq. (1)) and the pressure drop in the system is the same with total flow resistance (Δp_g, as illustrated in Eq. (4)).

A dimensionless number X is defined as the ratio of the total driving force (Δp_t) to the total pressure drop (Δp_g) in the system at a given heat flux:

$$\frac{\Delta p_t}{\Delta p_g}=X \tag{11}$$

where X represents the flow capability of the loop, which must be positively correlated with CHF. We assumed that the flow resistance in each component (the evaporator, rising tube, condenser, etc.) can be calculated by the Darcy-Wesbach formula using vapor density (liquid flow resistance is neglected). Then, defining u_i as velocity, d_i, l_i as the diameter, length, respectively, in the rising tube, whose subscript i represent dissimilar components such as the rising tube, condenser, and evaporator, etc. In diverse ranges of Re, the internal resistance calculation of the system and the derivation process of X are as follows.

(I) Laminar flow region

When the heat transfer load is low, we consider the laminar flow of the gas working fluid in the loop here. On the basis of Eq. (6), the following series of equations can be derived:

$$Re_i=\frac{\rho_g u_i d_i}{\mu_g}=\frac{Q d_i}{\mu_g \gamma A_i}=\frac{4Q}{\mu_g \gamma \pi d_i} \tag{12}$$

$$\frac{\Delta p_t}{\Delta p_g}=X=\frac{(\rho_l-\rho_g)gH}{\frac{1}{2}\Sigma_{i=1}^{n} f_i\frac{l_i}{d_i}\rho_g u_i^2}=\frac{\rho_l gH}{\Sigma_{i=1}^{n}\frac{1}{2}f_i\frac{l_i}{d_i}\rho_g\left(\frac{4Q}{\gamma\rho_g\pi d_i^2}\right)^2}$$

$$=\frac{\pi gH}{\Sigma_{i=1}^{n}(2C_i d_i^{-4}Q l_i)}\frac{\rho_g\rho_l\gamma}{\mu_g} \tag{13}$$

where C_i is a constant to calculate Darcy friction factor. The right side of Eq. (13) can be divided into two items. Specifically, the first item is correlated with the structure of the LGHP, written as $\frac{\pi gH}{\Sigma_{i=1}^{n}(2C_i d_i^{-4}Q l_i)}$, while the other is only associated with to the property parameters of the working fluid, namely, $\frac{\rho_g\rho_l\gamma}{\mu_g}$, defined as a two-phase composite physical parameter (M):

$$M=\frac{\rho_g\rho_l\gamma}{\mu_g} \tag{14}$$

(II) Smooth turbulent flow region

In most cases, the vapor flow in the loop with critical heat flux will get into the turbulent flow region. The turbulent flow region can be divided into three parts: smooth turbulent region, transitional rough turbulent region, and fully rough turbulent region. The smooth turbulent region is analyzed here by adopting Eq. (7),

$$\frac{\Delta p_t}{\Delta p_g}=X=\frac{(\rho_l-\rho_g)gH}{\frac{1}{2}\Sigma_{i=1}^{n} f_i\frac{l_i}{d_i}\rho_g u_i^2}=\frac{\rho_l gH}{\Sigma_{i=1}^{n}\frac{1}{2}f_i\frac{l_i}{d_i}\rho_g\left(\frac{4Q}{\gamma\rho_g\pi d_i^2}\right)^2}$$

$$=\frac{\sqrt{2}\pi^{1.75}gH}{\Sigma_{i=1}^{n}(8C_i d_i^{-4.75}Q^{1.75}l_i)}\frac{\rho_g\rho_l\gamma^{1.75}}{\mu_g^{0.25}} \tag{15}$$

The right side of Eq. (15) also contains two items: $\frac{\sqrt{2}\pi^{1.75}gH}{\Sigma_{i=1}^{n}(8C_i d_i^{-4.75}Q^{1.75}l_i)}$ and $\frac{\rho_g\rho_l\gamma^{1.75}}{\mu_g^{0.25}}$. To be specific, the first item is also correlated with the structure, while the other is only bound up with the property parameters of the working fluid, which we write as a two-phase composite physical parameter (J) [31],

$$J=\frac{\gamma^{1.75}\rho_g\rho_l}{\mu_g^{0.25}} \tag{16}$$

(III) Fully rough turbulent flow region

In this region, f can be calculated by adopting Eq. (12) and Eq.

(17),

$$f_i=\left[2\lg\left(\frac{\varepsilon_i/d_i}{3.7}\right)\right]^{-2} \quad (17)$$

$$\frac{\Delta p_t}{\Delta p_g}=X=\frac{(\rho_1-\rho_g)gH}{\frac{1}{2}\Sigma_{i=1}^{n}f_i\frac{l_i}{d_i}\rho_g u_i^2}=\frac{\rho_l gH}{\Sigma_{i=1}^{n}\frac{1}{2}f_i\frac{l_i}{d_i}\rho_g\left(\frac{Q}{\gamma\rho_g A_i}\right)^2}$$

$$=\frac{\pi^2 gH}{\Sigma_{i=1}^{n}(8f_i d_i^{-5}Q^2 l_i)}\rho_g\rho_1\gamma^2 \quad (18)$$

In Eq. (18), the item $\rho_g\rho_1\gamma^2$ is represented by N,

$$N=\rho_g\rho_1\gamma^2 \quad (19)$$

(IV) Transitional rough turbulent flow region

In this region, f is difficult to express directly. As a consequence, the two-phase physical parameter of the transitional rough turbulent flow will be investigated on the basis of J and N.

In terms of a given LGHP, the mechanical structure is fixed. In accordance with Eqs. (13), (15) and (18), X will heighten as two-phase composite physical parameters (M, J, N) rise in the corresponding flow region. To put it in another way, the working fluid with a higher value of M, J, N can make the system work at a higher driving force and have a higher heat transfer limit (CHF).

Concentrating on the turbulent flow region, some experiments were subsequently carried out to verify the conclusion.

EXPERIMENTAL SETUP

1. Experimental Apparatus

As depicted in Fig. 1, the experimental system consists of an LGHP, an auxiliary heating system, and a data acquisition system. The condenser is positioned 1.8 m above the evaporator. Apart from that, all the pipelines are copper tubes, and other detailed parameters are illustrated in Table 2. The system is covered by 10 mm thick thermal insulation material and a thermal conductivity of 0.035 W/(m·°C) to lessen heat loss. The system employs a check valve to ensure the directional movement of the working fluid in the LGHP to prevent reverse flow. More detailed descriptions of each part are given below.

(1) Evaporator: The flat evaporator is the core part of the system that determines the heat transfer performance of the system [32]. Fig. 2(a) displays the the internal structure of the flat evaporator. The specific parameters are depicted in Table 2. The evaporator inlet and outlet are at the bottom of the

Table 2. Geometric characteristics of experimental LGHP

Parameter	Value/mm	Parameter	Value/mm
Heating block		**Inlet tube**	
Overall dimensions	120×120×50	Diameter (outlet/inlet)	8.5/6.35
Heating rod size	100×10Φ	Length	53
Heating rod number	12	**Outlet tube**	
Evaporator		Diameter (outlet/inlet)	8.5/6.35
Overall dimensions	140×120×21	Length	65
Top wall thickness	3	**Upward tube**	
Bottom wall thickness	3	Diameter (outlet/inlet)	10/6.5
Side wall thickness	5.5	Length	2,100
Square column size	3×3×15	**Downward tube**	
Inter-column distance	3	Diameter (outlet/inlet)	10/6.5
		Length	1,800

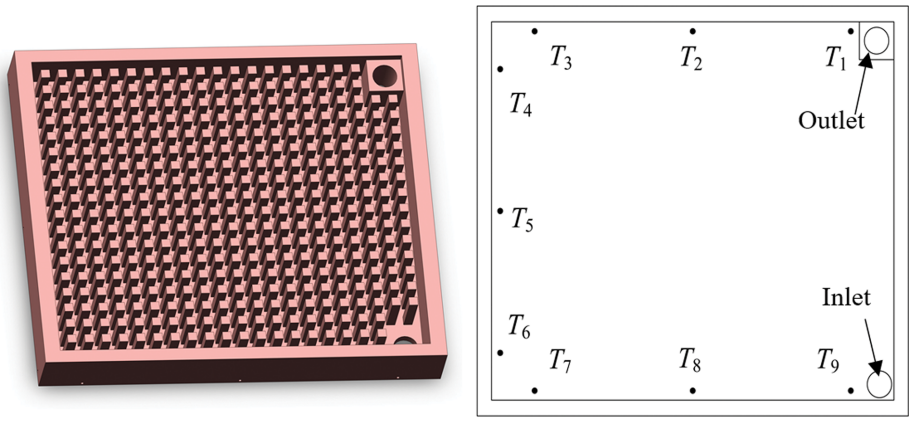

(a) (b)

Fig. 2. (a) Internal structure of the flat plate evaporator, (b) Temperature measurement points of the evaporator.

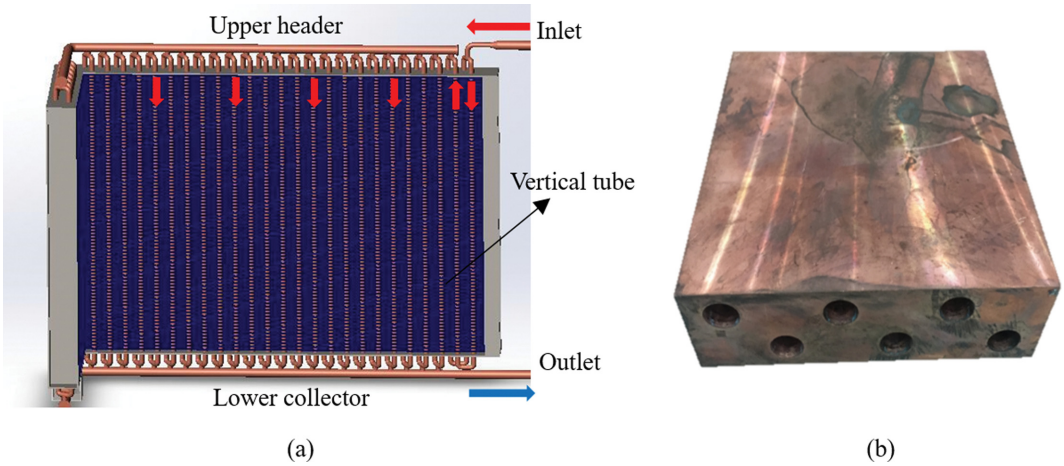

Fig. 3. (a) Structure of the falling tube condenser, (b) Cooper heating block.

evaporator. A multitude of square columns are distributed throughout the evaporator and connected with the top and bottom surfaces of the evaporator by using a special welding method. This structure is advantageous in two facets: above all, it can enlarge the heat transfer area and effectively conduct heat from the bottom to the top wall. Aside from that, uniform temperature across the evaporator can be materialized; furthermore, this structure can withstand higher pressure.

(2) Condenser: To decrease the pressure drop, a vertical tube condenser was used [33]. As exhibited in Fig. 3(a), a U-tube is present at the condenser inlet; the superheated working fluid vapor flows through the U-tube and is distributed to 60 parallel vertical tubes at the upper header. Subsequently, the condensed liquid flows down along the vertical tubes and the liquid sealing device to the falling tube. Tests confirmed that the pressure drop in this condenser is extremely small.

(3) Heating block: A copper block is employed as the heating device. As depicted in Fig. 3(b), twelve cartridge heaters are inserted inside the copper block to provide a heat load of 3,600 W. The copper heating block is directly in contact with the flat plate evaporator. Apart from that, thermal silicone grease is used to ensure favorable thermal contact between the bottom of the evaporator and the upper surface of the heating block.

(4) Data acquisition system: As described in Fig. 2(b), nine T-type thermocouples are first placed 1.5 mm below the internal surface of the evaporator. Subsequently, they are inserted into the baseboard. Due to the limitation of processing technology, the temperature measuring hole with diameter of 1 mm can only be drilled to a depth of 15 mm. Afterwards, two absolute omega pressure sensors were used for the absolute pressure at the evaporator inlet and outlet. The temperature and pressure signals are monitored and transformed into voltages, and subsequently collected by the HP 34901A multiplexer.

2. Data Processing

The heat flux (q) is equal to the ratio of the input heat load (Q) to the heating area (A) between the evaporator and the heating block:

$$q = \frac{Q}{A} \tag{20}$$

The average wall temperature (T_a) at the measuring point and the evaporator internal surface temperature (T_w) can be calculated by adopting Eq. (21) and (22).

$$T_a = \frac{1}{9}\Sigma_1^9 T_i \tag{21}$$

$$T_w = T_a - \frac{q\delta}{\lambda} \tag{22}$$

Thermal grease is applied evenly between the evaporator and the heating block, and the two parts are pressed together tightly and secured with bolts. Therefore, the contact thermal resistance is considered to be negligible.

The evaporation of the working fluid in the evaporator can be regarded as pool boiling; therefore, the pressure drop in the evaporator is small, and the evaporating pressure is assumed to be equal to the average of the inlet and outlet pressures. Thus, the temperature of the liquid working fluid is approximately equal to the saturation temperature T_s, which can be calculated from the saturation pressure p_s,

$$p_e = \frac{p_{ei} + p_{eo}}{2} \tag{23}$$

$$T_s = f(p_s) \tag{24}$$

In this experiment, ΔT is defined as the difference of temperature between the internal surface and the working fluid:

$$\Delta T = T_w - T_s = \frac{T_1 + T_2 + \cdots + T_9}{9} - \frac{Q\delta}{A\lambda} - f\left(\frac{p_{ei} + p_{eo}}{2}\right) \tag{25}$$

The heat transfer coefficient is defined as:

$$h = \frac{q}{\Delta T} \tag{26}$$

3. Uncertainty and Heat Loss

All the pressure sensors and thermocouples were calibrated by high precision sensor probes. Uncertainty analysis of the experimental data was performed by adopting the root sum square method

Table 3. Uncertainties for dissimilar parameters involved in the experimental tests

Parameter	Measurement instrument	Uncertainty (confidence coefficient k=2)
T/°C	T-type thermocouple (TT-T-30)	±0.126 °C
p/Pa	Pressure sensor (BST6600)	±682 Pa
Filling amount/g	Electronic balance (ACS030M/C-D)	±2.0 g
Q/W	Power transducer (WBP112S91)	±5.18 W

[34]. Table 3 displays the uncertainties associated with the parameters of the experimental apparatus used in this study.

According to the Moffat formula and Eq. (26), the uncertainty formula Eq. (27) and Eq. (28) were derived:

$$u_{\Delta T}=\left\{\Sigma_1^{10}\left(\frac{1}{10}u_{T_i}\right)^2+\left(\frac{\delta}{A\lambda}u_Q\right)^2+\left[\frac{1}{2}f'(p)\right]^2\left(u_{p_{ei}}^2+u_{p_{eo}}^2\right)\right\}^{\frac{1}{2}} \quad (27)$$

$$u_h=\left\{\left[\frac{1}{A\Delta T}u_Q\right]^2+\left[\frac{Q}{A(\Delta T)^2}u_{\Delta T}\right]^2\right\}^{\frac{1}{2}} \quad (28)$$

where u_h is the uncertainty of heat transfer coefficient, and u_Q and $u_{\Delta T}$ are the uncertainty of heating power and temperature difference of heat transfer. Since the working pressure range of the experiment is 0.2-1.5 MPa, the relative uncertainty of the heat transfer coefficient of the experiment is 4.24% (confidence probability 95%) by using 0.85 MPa as average pressure.

The evaporator and heat sources were insulated by the thermal insulation material. The thickness of the thermal insulation material was 10 mm, the surface area was 0.08 m^2, and the conductivity coefficient was 0.035 W/(m·°C). When the input heat power was 1,500 W, the temperature difference inside and outside the insulation materiall was 40 °C. The heat loss can be calculated by Eq. (29):

$$\frac{Q_{loss}}{Q}=\frac{\lambda A\frac{\Delta t}{\delta}}{Q}=\frac{0.035\times 0.08\times\frac{40}{0.01}}{1{,}500}=0.747\% \quad (29)$$

The heat loss is less than 1%, approximately adiabatic.

4. Experimental Process

In this experimental study, the CHF of the tested working fluids was measured. To be specific, the ambient temperature temperature was 23 °C. When the system was stable, the temperature fluctuation at each probe was less than 0.5 °C over 5 min. The tests were repeated in triplicate to ensure the consistency and reproducibility of the experiment. The experimental procedure involved multiple steps as follows:

(1) A leakage check was performed to ensure that the system maintains consistent performance over time. Initially, at 2 MPa, the pressure of the closed system was found to lessen by only 0.02 MPa after 24 h, which is considered to be an acceptable amount of leakage.

(2) The inside of the system was degassed by employing a vacuum pump. Afterwards, the volume of the system (V_{sys}) could be measured by charging nitrogen. Then, the system was degassed again, and a steel cylinder for storing the working fluid was inverted and placed on an electronic scale. Subsequently, the working fluid was charged into the system. By recording the change in the number of the electronic scale, the mass of the working fluid charged into the system can be measured and combined with the pressure of the system measured by pressure sensors. The fill ratio (α) was defined as the ratio between the volume of the working fluid (V_{wf}) and the system (V_{sys}), as depicted in Eq. (30),

$$\alpha=V_{wf}/V_{sys} \quad (30)$$

for each working fluid, the fill ratio was set as a fixed value.

(3) The evaporator was then gradually heated by adopting the copper heating block. The input power was adjusted by changing the input voltage via the voltage regulator. The condenser used forced air convection to condense the working fluid. The temperature of the air was about 23 °C. All data were recorded when the system stabilized.

RESULTS AND DISCUSSION

1. Determination of the CHF and the Optimal Working Fluid Fill Ratio

To effectively determine the CHF, R134a was first selected for further investigations. Fig. 4 exhibits the temperatures (T_1-T_9) of the heated wall. Subsequently, the test proceeded by increasing the heat input in small increments, each followed by an adequate waiting period. Temperatures increased gradually to steady-state levels. Eventually, when reaching a certain heat flux density, the temperature near the evaporator outlet of the heated wall (T_1 and T_2) increased suddenly, which exceeded the safe temperature of electronic equipment (65 °C) [35] and had no sign of temperature drop, which was more than the safe temperature of electronic equipment. Such circumstance meant the outlet of the evaporator exhibited signs of drying up and the heat transfer performance was lessened. As a result, this heat flux density can be defined as CHF, as exhibited in Fig. 4.

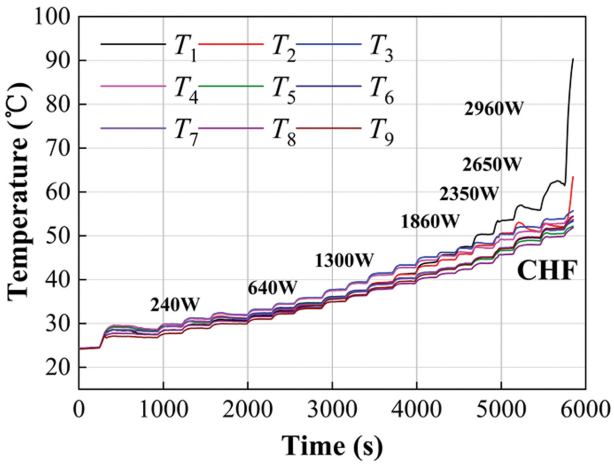

Fig. 4. The wall temperature when adopting R134a.

Table 4. CHFs and physical parameter of tested working fluids

Working fluid	CHF (kW/m^2)	P_e (kPa)	T (°C)	Re	$M=\rho_g\rho_l\gamma/\mu_g$ $\times10^{-14}$ ($J\cdot s\cdot m^{-5}$)	$J=\gamma^{1.75}\rho_g\rho_l/\mu_g^{0.25}$ $\times10^{-14}$ ($J^{1.75}\cdot s^{0.25}\cdot m^{-5.75}$)	$N=\rho_g\rho_l\gamma^2$ $\times10^{-14}$ ($J^2\cdot m^{-6}$)
R245fa	113.750	214.557	35.39	110,343	2.721	2.559	5.400
R600a	128.472	472.144	35.58	100,247	2.661	2.945	6.564
R142b	139.750	494.681	38.01	128,267	4.181	4.097	8.768
R124	143.736	572.751	38.72	164,209	5.207	4.330	8.773
R290	177.431	1,475.480	43.26	125,773	5.009	5.958	13.601
R134a	188.750	984.647	38.81	179,610	7.440	7.097	15.050
R152a	199.132	903.527	39.76	138,218	5.904	7.135	16.373
R22	203.882	1,500.835	39.12	175,992	9.228	9.469	20.577

The insufficient working fluid in the rising tube diminishes the driving force generated by the density difference between the liquid and vapor forms of the working fluid, and may result in the fail start-up of the system. As a result, tests were conducted to determine the optimal fill ratio before the principal experiment was carried out. The CHF of R134a was measured under distinct fill ratios ranging from 10-65%. When the working fluid fill ratio was less than 25%, the loop system failed to start. CHF increases with the augment of filling rate, with a variation range of 25-40%. Nonetheless, when the fill ratio was greater than 40%, the CHF no longer increased with the increased fill ratio. Consequently, an optimal fill ratio existed. In the subsequent experiments, the fill ratio was set to 50% in order to control variables and ensure the redundancy of the system.

2. Evaluation Criterion of Working Fluid in LGHPs

2-1. Evaporation Pressure

Traditionally, it is universally acknowledged that working fluids with higher evaporation pressure correspond to higher CHFs in LGHP. The same result holds true for this experiment. Apart from R134a, some other working fluids are tested to specify the correlation between the working fluid properties and CHF. It is noteworthy that the experimental processes are the same as the CHF test method of R134a in section 4.1. Table 4 illustrates the the experimental results of the CHF and evaporation pressure.

As clearly revealed in Table 4, the working fluids with higher evaporating pressures (R22, R290, R134a, R152a) generally enable the system to actualize a higher CHF, while the working fluids with lower evaporating pressures (R245fa, R600a, R142b, R124) give rise to worse performance. R22 reaches the highest CHF under the highest evaporating pressure among the working fluids tested. Nevertheless, R290 displays an exception. Comparing R290 with R134a and R152a, although the saturation pressure of R290 is the highest one, the CHF of R290 is the lowest. It turns out that higher evaporating pressure does not always result in a higher CHF. As a consequence, it's not a perfect evaluation criterion of working fluids in LGHPs. On that account, it's imperative to identify some more accurate criteria.

2-2. Composite Two-phase Physical Parameters

In accordance with the previous derivation in section 2.2, the composite two-phase physical parameters (M, J, N) are pivotal parameters that can be used to characterize the driving force and CHF. Table 4 compiles the CHF and two-phase physical parameters M, J, N of the working fluids tested, where M, J, N are calculated at the saturation temperature of working fluid when the wall temperature of the evaporator reaches nearly 65 °C.

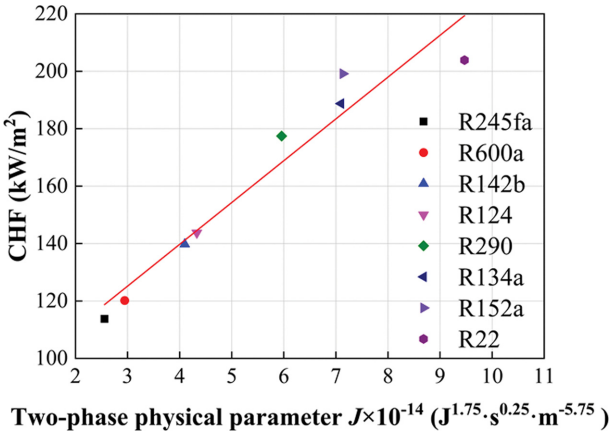

Fig. 5. Experimental results of CHF versus J.

As depicted in Table 4, when the system reaches its CHF, the Re is much larger than the Re of the laminar flow (Re<4,000). Hence, it is not accurate enough to use M to evaluate whether the working fluid can reach higher CHF in a certain LGHP. As illustrated in Table 4, there is no obvious linear correlation between M and CHF.

While in the smooth turbulent flow region ($4{,}000<Re<10^5$), the CHF increases as J increases and follows a linear relationship. The scatter plot in Fig. 5 depicts the experimental data points, and it is seen that there is a significant positive correlation between CHF and J, which corresponds to the theoretical analysis. As a result, the parameter J is more dependable than working pressure as a potential criterion for selecting an appropriate working fluid for LGHPs.

With regard to the rough turbulent flow region, it is difficult to find the boundary between the transitional rough turbulent flow region and the fully rough turbulent flow region. By first analyzing the fully rough turbulent Eq. (18), Re will no longer affect the friction factor in the flow process. Under this circumstance, parameter N is merely associated with ρ_g, ρ_l, γ. Moreover, the CHF not only heightens as N increases, but also follows a more conspicuous linear relationship as exhibited in Fig. 6, which also coincides with the theoretical analysis. As a consequence, parameter N can also be employed as a potential criterion for the selection of the working

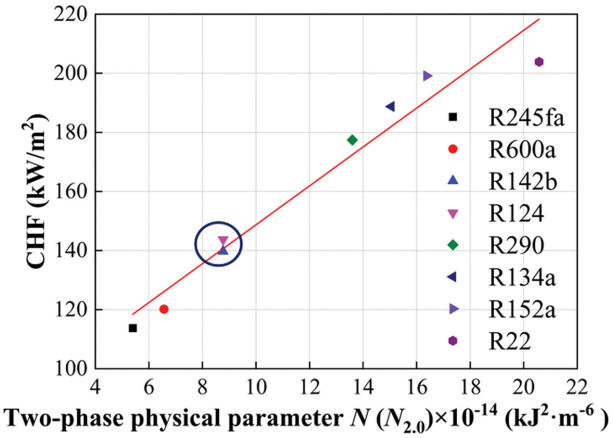

Fig. 6. Experimental results of CHF versus N.

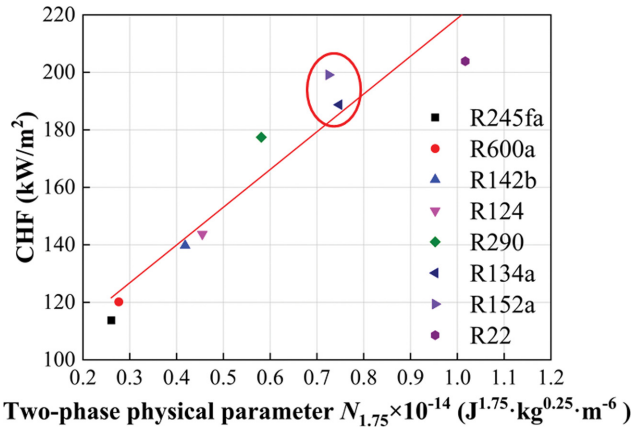

Fig. 7. Experimental results of CHF versus $N_{1.75}$.

fluid in LGHP.

Apart from that, all the Re is slightly larger than 10^5 when the system reaches CHF in the experimental results. They may fall into the transitional rough turbulent flow region. Consequently, it is essential to conduct further analysis.

In the smooth turbulent flow region and the fully rough turbulent flow region, the composite two-phase physical parameters are $J=\rho_g\rho_l\gamma^{1.75}\mu_g^{-0.25}$, $N=\rho_g\rho_l\gamma^2$, respectively. Nevertheless, for most of the working fluids used in the experiment, their viscosity (μ_g) is tremendously similar when reaching CHF. As displayed in Table 5, the values of $\mu_g^{-0.25}$ are almost equal. Consequently, we neglect the effect of $\mu_g^{-0.25}$ in J evaluation parameter. To compare J and N more intuitively, a new two-phase physical parameter $N_{1.75}$ is derived,

$$N_{1.75}=J\cdot\mu_g^{0.25}=\rho_g\rho_l\gamma^{1.75} \tag{31}$$

And rewrite N as $N_{2.0}$,

$$N_{2.0}=N=\rho_g\rho_l\gamma^2 \tag{32}$$

As clearly exhibited in Table 5, $N_{1.75}$ still follows an approximately linear relationship with CHF. In summary, it can be assumed that the two-phase physical parameter N_n in the transitional rough turbulent flow region is between $N_{1.75}$ and $N_{2.0}$, which can be written as,

$$N_n=N=\rho_g\rho_l\gamma^n\ (1.75<n\le 2.0) \tag{33}$$

Table 5. Physical parameters and viscosity of tested working fluids

Working fluid	CHF (kW/m^2)	$\mu_g\times10^6$ ($Pa\cdot s$)	$\mu_g^{0.25}$ ($Pa^{0.25}\cdot s^{0.25}$)	$J=\gamma^{1.75}\rho_g\rho_l/\mu_g^{0.25}$ $\times10^{-14}$ ($J^{1.75}\cdot s^{0.25}\cdot m^{-5.75}$)	$N_{1.75}=\rho_g\rho_l\gamma^{1.75}$ $\times10^{-14}$ ($J^{1.75}\cdot kg^{0.25}\cdot m^{-6}$)
R245fa	113.750	10.7826	0.057303	2.559	0.261
R600a	128.472	7.7856	0.052823	2.945	0.277
R142b	139.750	10.8700	0.057419	4.097	0.418
R124	143.736	12.1948	0.059094	4.330	0.455
R290	177.431	9.0475	0.054844	5.958	0.581
R134a	188.750	12.3144	0.059238	7.097	0.748
R152a	199.132	10.6555	0.057134	7.135	0.725
R22	203.882	13.3033	0.060393	9.469	1.017

Table 6. CHFs and composite two-phase physical parameters of tested working fluids

Working fluid	CHF (kW/m^2)	$N_{1.75}=\rho_g\rho_l\gamma^{1.75}$ $\times10^{-14}$ ($J^{1.75}\cdot kg^{0.25}\cdot m^{-6}$)	$N_{2.0}=\rho_g\rho_l\gamma^2$ $\times10^{-14}$ ($J^2\cdot m^{-6}$)	$N_{1.875}=\rho_g\rho_l\gamma^{1.875}$ $\times10^{-14}$ ($J^{1.875}\cdot kg^{0.125}\cdot m^{-6}$)
R245fa	113.750	0.261	5.400	1.187
R600a	128.472	0.277	6.564	1.348
R142b	139.750	0.418	8.768	1.915
R124	143.736	0.455	8.773	1.998
R290	177.431	0.581	13.601	2.811
R134a	188.750	0.748	15.050	3.354
R152a	199.132	0.725	16.373	3.445
R22	203.882	1.017	20.577	4.575

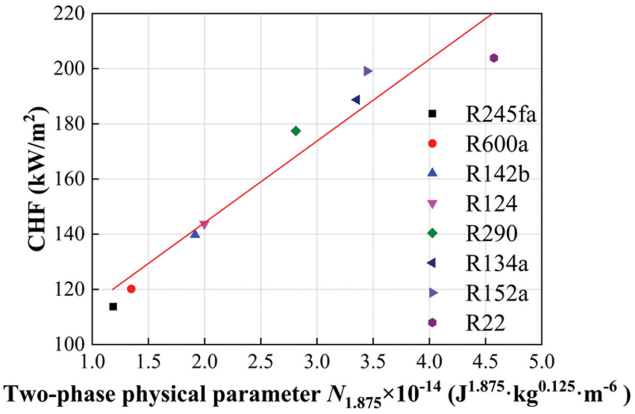

Fig. 8. Experimental results of CHF versus $N_{1.875}$.

As displayed in Fig. 7 and Table 6, if adopting $N_{1.75}$ to select the working fluid for the system, the CHF of R134a is less than R152a in experiments while the $N_{1.75}$ of R134a is larger than R152a, which not follows a monotonically increasing relationship. In other words, $N_{1.75}$ eliminates the effect of viscosity, which resulted in the $N_{1.75}$ value of R134a being greater than R152a. To put it in another way, $N_{1.75}$ may make something wrong in evaluating CHF of the working fluid with a higher value of $N_{1.75}$.

Moreover, as evidently displayed in Fig. 6 and Table 6, when adopting $N_{2.0}$ to select the working fluid for the system, the $N_{2.0}$ of R142b and R124 are considerably close, while there is a certain difference between their CHF. As a result, $N_{2.0}$ neither done well enough in evaluating CHF of the working fluid with a lower value of $N_{2.0}$.

Since viscosity no longer played a role in the pressure drop calculation formula in the fully rough turbulent flow region, and the values of $\mu_g^{-0.25}$ of different working fluids in smooth turbulent flow region were very close. For the sake of getting a more accurate composite two-phase physical parameter, by considering the characteristics of both $N_{1.75}$ and $N_{2.0}$, the average value of the upper and lower limit for n, i.e. n=1.875, is used. Afterwards, the two-phase physical parameter in the transitional rough turbulent flow region can be written as,

$$N_{1.875}=\rho_g\rho_l\gamma^{1.875} \tag{34}$$

As exhibited in Fig. 8, there is a monotonically increasing correlation between CHF and $N_{1.875}$, and the linearity between $N_{1.875}$ and CHF is more well-distributed by comparing with $N_{1.75}$ and $N_{2.0}$. Thus, when Re enters in the turbulent flow region, if we cannot identify which region the flow state will be, $N_{1.875}$ should be a more trustworthy evaluation criterion for working fluid choosing for an LGHP.

CONCLUSION

We investigated the correlation between the properties of the working fluid and the CHF in an LGHP system. A dimensionless number, X, and some composite two-phase physical parameters were derived. Experiments were conducted by adopting diverse working fluids to get the CHFs and study the evaluation criterion of working fluids in LGHPs. A two-phase physical parameter $N_{1.875}$ was derived by taking the average value of exponential index n of $N_{1.75}$ with $N_{2.0}$, which exhibits a linear correlation with the CHF measured in the experiments. Comparing $N_{1.75}$ with $N_{2.0}$, we recommend $N_{1.875}$ as an evaluation criterion in working fluid choice for LGHP.

ACKNOWLEDGEMENTS

This work was supported by National Natural Science Foundation of China (51976063) and Natural Science Foundation of Guangdong Province, China (2019A1515011253).

NOMENCLATURE

A : heating area [mm²]
c_T : specific heat at constant temperature [kJ·kg⁻¹·°C⁻¹]
d : internal diameter of tube [mm]
g : acceleration of gravity [m·s⁻²]
f : Darcy friction factor
H : height difference [mm]
l : distance [mm]
$\dot{m}$: mass flow rate [kg·s⁻¹]
p : pressure [kPa]
Q : heat load [W]
q : heat flux [W·m⁻²]
Re : Reynolds number
T : temperature [°C]
v : velocity [m·s⁻¹]
V : volume [m³]
M, J, N, $N_{1.75}$, $N_{1.875}$, $N_{2.0}$: two-phase physical parameter

Greek Symbols

α : fill ratio
Δ : increment, standard deviation
λ : conductivity coefficient [W·m⁻¹·°C⁻¹]
μ_g : dynamic viscosity [Pa·s]
δ : thickness [mm]
ρ : density [kg·m⁻³]
γ : latent heat [J·kg⁻¹]
ε : roughness

Subscripts

a : temperature measuring point
e : evaporator
ei : evaporator inlet
eo : evaporator outlet
g : gas
l : liquid
sys : system
t : total
w : wall
wf : working fluid

REFERENCES

1. R. E. Simons and R. C. Chu, *IEEE*, 1 (2000).
2. B. Agostini, M. Fabbri, J. E. Park, L. Wojtan, J. R. Thome and B. Michel, *Heat Transfer Eng.*, **28**, 258 (2007).

3. P. H. Chen, S. W. Chang, K. F. Chiang and J. Li, *Recent Patents on Engineering*, **2**, 174 (2008).
4. Y. F. Maidanik, Y. G. Goncharov and K. A. Fershtater, *ESA Special Publication*, **1** (1991).
5. D. Khrustalev, *IEEE*, 145 (2002).
6. J. Li, D. M. Wang and G. P. B. Peterson, *IEEE Transactions on Components, Packaging and Manufacturing Technology*, **1**, 519 (2011).
7. C. Sarno, C. Tantolin, R. Hodot, Y. Maydanik and S. Vershinin, *Appl. Therm. Eng.*, **51**, 764 (2013).
8. G. H. Zhou, J. Li and L. C. Lv, *Appl. Therm. Eng.*, **109**, 514 (2016).
9. R. Khodabandeh, *Appl. Therm. Eng.*, **24**, 2643 (2004).
10. A. Samba, H. Louahlia-Gualous, S. Le Masson and D. Nörterhäuser, *Appl. Therm. Eng.*, **50**, 1351 (2013).
11. C. C. Chang, S. C. Kuo, M. T. Ke and S. L. Chen, *Exp. Heat Transfer*, **23**, 144 (2010).
12. S. H. Noie, *Appl. Therm. Eng.*, **25**, 495 (2005).
13. L. L. Vasiliev, *Appl. Therm. Eng.*, **25**, 1 (2005).
14. L. Z. Bai, J. H. Guo, G. P. Lin, J. He and D. S. Wen, *Appl. Therm. Eng.*, **83**, 88 (2015).
15. L. Z. Bai, G. P. Lin and H. X. Zhang, *Acta Aeronautica et Astronautica Sinica*, **29**, 1112 (2008).
16. P. L. Zhang, X. T. Li, S. Shang, W. X. Shi and B. L. Wang, *International Refrigeration and Air Conditioning Conference*, 2519 (2014).
17. Z. H. Liu, X. F. Yang, G. S. Wang and G. L. Guo, *Int. J. Heat Mass Tran.*, **53**, 1914 (2010).
18. S. G. Liter and M. Kaviany, *Int. J. Heat Mass Tran.*, **44**, 4287 (2001).
19. R. Khodabandeh, *Int. J. Refrig*, **28**, 190 (2005).
20. R. Khodabandeh and B. Palm, *Int. J. Therm. Sci.*, **41**, 619 (2002).
21. Z. Li and R. H. S. Winterton, *Int. J. Heat Mass Tran.*, 2759 (1991).
22. M. Cooper, *Advances in Heat Transfer*, 157 (1984).
23. J. J. He, J. P. Liu and X. W. Xu, *Int. J. Heat Mass Tran.*, **105**, 452 (2017).
24. G. Kocamustafaogullari and M. Ishii, *Int. J. Heat Mass Tran.*, **26**, 1377 (1983).
25. K. Zhu, X. Q. Li, H. L. Li, X. Q. Chen and Y. B. Wang, *Appl. Therm. Eng.*, **130**, 354 (2018).
26. A. Franco and S. Filippeschi, *Exp. Therm. Fluid Sci.*, **51**, 302 (2013).
27. J. W. Chen, W. B. Huang, J. W. Cen, W. J. Cao, Z. B. Li, F. Li and F. M. Jiang, *Energy*, **255**, 124531 (2022).
28. R. Singh, T. Nguyen, M. Mochizuki and A. Akbarzadeh, *Therm. Sci. Eng. Prog.*, **35**, 101451 (2022).
29. Y. D. Guo, G. P. Lin, J. He, H. X. Zhang, J. Y. Miao and J. D. Li, *Appl. Therm. Eng.*, **155**, 267 (2019).
30. R. W. Fox and A. T. Mcdonald, *Mech. Eng.*, **35**, 7 (1973).
31. L. J. Liang, J. P. Liu and X. W. Xu, *J. Chem. Ind. Eng. (China)*, **69**, 4231 (2018).
32. Y. F. Maydanik, *Appl. Therm. Eng.*, **25**, 635 (2005).
33. J. G. Ruan, J. P. Liu, X. W. Xu, J. X. Chen and G. L. Li, *Appl. Therm. Eng.*, **140**, 325 (2018).
34. R. J. Moffat, *Exp. Therm. Fluid Sci.*, **1**, 3 (1988).
35. G. Yao, Z. Ma, L. Luo and R. Chen, *J. Jiangsu Univ. Sci. Technol. (Natural Science Edition)*, **17**, 9 (2003).